Journal of Power Sources 180 (2008) 748–754

Contents lists available at ScienceDirect

Journal of Power Sources

journal homepage: www.elsevier.com/locate/jpowsour

A multi-instrumented polymer exchange membrane fuel cell: Observation of the in-plane non-homogeneities

Gaël Maranzana*, Olivier Lottin, Thibaut Colinart, Sylvain Chupin, Sophie Didierjean

LEMTA, Nancy-University, CNRS, 2 avenue de la Forêt de Haye, B.P. 160, 54504 Vandoeuvre lès Nancy Cedex, France

ARTICLE INFO

Article history:
Received 6 December 2007
Received in revised form 1 February 2008
Accepted 1 March 2008
Available online 8 March 2008

Keywords:
Fuel cell
Local current
Local temperature
Liquid water observation
Aging

ABSTRACT

A multi-instrumented single polymer exchange membrane fuel cell is tested. It allows measuring local current densities and the temperature field along the gas channels. It is built from transparent PMMA so that an additional observable is the location where liquid water appears in the channels. Some local and transient observations are presented. A result is that the temperature field is strongly correlated with the current density distribution and it is confirmed that both depend strongly on water management. Some local aging effects and the observation of internal currents in open circuit conditions are reported.

1. Introduction

The electrodes of proton membrane exchange fuel cells (PEMFCs) are fed by gases, whose properties are changing during their progress from the inlet to the outlet of the channels. For instance, the reactant concentration decreases and the water concentration increases. The total pressure diminishes, the temperature is dependent on the local current density, and liquid water may appear, or disappear. The electrode performance is not uniform, which can have consequences on the global performances of the cell or on its durability. The purpose of this paper is to report the experimental observation of these non-homogeneities. For this, a dedicated multi-instrumented single PEM fuel cell was designed and built. It allows measuring both current density and temperature fields along the gas channels. It is made of transparent polymethyl methacrylate (PMMA) so that an additional observable is the location of liquid water in the channels.

Several authors thought already of building an experimental setup allowing to measure the local current distribution in the plane of a cell. Cleghorn et al. [1] used a printed circuit board (PCB) to segment the anode current collector and flow field of a 100 cm^2 cell. According to them, this technology may provide a number of advantages, including the relatively cheap and rapid manufacture of a wide range of segment patterns. High stoichiometry tests show some fabrication-dependent variations in current from segment to segment. They may be explained by differences in interfacial contacts between catalyst layer, gas diffusion backing and current collector, or by the variability of the catalyst layer performance. These variations are in the order of 100 mA cm^{-2} at 0.7 V or 300 mA cm^{-2} at 0.2 V. Recently, Brett et al. [2] took up this PCB technique to build a single channel cell without segmenting the backing layers. They used Nafion 112 instead of Nafion 117 and their conclusions qualitatively endorse the findings of Cleghorn et al. However, they found a disparity in the correlation between current and electrode resistance: the electrode resistance does not increase at higher current as Cleghorn et al. noticed. This fact can be attributed to the use of a thinner membrane that is less subjected to drying.

Stumper et al. [3] describe three different techniques for the determination of the current density distribution in operating fuel cells. They compare their relative benefits with respect to ease of implementation and information gain.

1. The "partial membrane electrode assembly (MEA) method" consists in testing independently portions or segments of MEA by masking areas or by making several partially catalyzed MEAs.
2. The "subcell" method allows the determination of localized currents in a full scale operational cell. Several isolated subcells are placed at conveniently chosen locations in the MEA.
3. The "current mapping method" can be considered as a generalization of the preceding one: it involves the use of a resistance

* Corresponding author. Tel.: +33 3 83 59 55 48; fax: +33 3 83 59 55 51.
E-mail address: gael.maranzana@ensem.inpl-nancy.fr (G. Maranzana).

0378-7753/$ – see front matter © 2008 Elsevier B.V. All rights reserved.
doi:10.1016/j.jpowsour.2008.03.002

network in order to map the current density. The main difficulty is that each segment has to be electrically isolated.

Stumper et al. conclude that these methods are particularly relevant for the optimization of water management and reactant distribution over the active area.

Mench et al. [4] constructed an electrically segregated flowfield by embedding current collecting ribs in a polycarbonate slab. The ribs were arranged to produce a single-pass serpentine flowfield. The advantage of this method is the low contact resistance between the ribs and the backing layer, which dispenses with the use of a segmented MEA and preserves true fuel cell operation characteristics. Experimental results show the high sensibility of the current density to the cathode flow rate and they put forwards the high characteristic time for cathode flooding by comparison with other transport and electrochemical phenomena. Sun et al. [5] developed a measuring gasket that was inserted between the flow field plate and the gas diffusion layer. This simple technique does not require specifically designed fuel cells or modification of the collector plates. The authors investigated the effects of airflow rates, hydrogen flow rates, humidification temperatures, operating temperatures and operating pressures. They used 23 measuring strips plated with gold. However, with this technique the MEAs are not segmented: thus, because of the contact resistance between the gold strip and the GDL, or of the own resistance of the strips, there is an uncertainty about the location where the current collected by a strip is produced.

Recently, Schulze et al. [6] described three different techniques used at the DLR Institute in Stuttgart for the measurement of the local current density. One technique is based on individual segments externally connected with resistances. The authors pointed out technical difficulties for positioning each segment horizontally in order to get uniform contact resistance. They also tested Hall effect sensors for non-intrusive measurements but report technical difficulties and high cost. Finally, they used successfully the Cleghorn's PCB technique. A drawback of this technology is the electrical resistance between each segment and the point where they are put to the same potential. Because of this resistance, if the current is different from one segment to other, the potential of the segments are not uniform.

The originality of the setup presented in this paper is to allow measuring two coupled local quantities: the current density and the temperature. Furthermore, the location of liquid water in the channels is an additional observable. This can prevent from misinterpretation of the global results. The geometry of the cell is voluntary kept simple in order to limit the complexity of anodic and cathodic flows and to facilitate the comparison with numerical results [7]. As a consequence, this cell does not always behave like a commercial one but it can help understanding fundamental principles and validating the results of some models.

2. Experimental setup

The cell is depicted in Fig. 1. Gas distribution is made through five 300-mm straight parallel channels of 1 mm × 1 mm in section. The plates are made of PMMA, which is transparent but non-conductive. The MEA (Nafion 115; 0.5 mgPt cm^{-2} on both anode and cathode) is manufactured by Paxitech (www.paxitech.com). On the anode side, the GDL is divided into 20 1.4-cm successive segments isolated by a 1-mm gasket and electrically connected only after current measurement. The electrodes are not segmented. The current collection is realized through perimetric gold wires: 2 for the cathode side and 40 (2 per segment which are then connected together) for the anode side. The wires are constricted between the backing

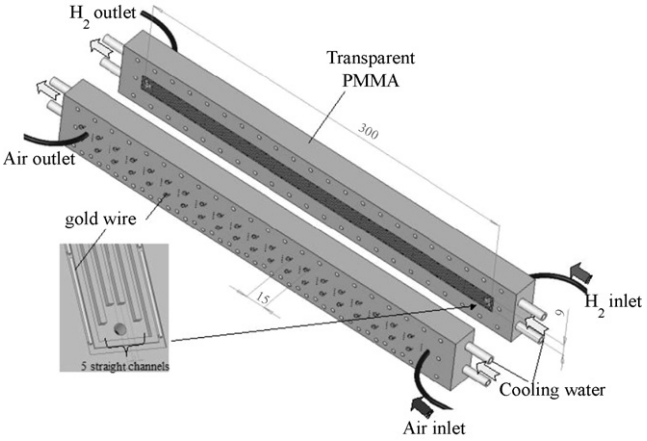

Fig. 1. Schematic view of the cell (dimensions are in millimeter).

layer and the plate. They pass through 20 Hall effect sensor (1 per segment) and are then connected to the same potential as shown in Fig. 2. Since the electrical resistance of gold wires and of connections is negligible (measured lower than 1 mΩ), it is reasonable to assume that the wire potentials are all identical at the interface with the backing layer. However, this does not guarantee that the 20 electrodes are strictly at the same potential because of the contact resistance between the wires and the GDL. So, a non-uniform current density may yield a non-uniform in-plane potential field. Moreover, the electrons being collected on the edge of the GDL, they must flow across the GDL at right angles to the gas flow. The resulting electrical resistance is of the order of:

$$R_{\parallel} = \rho\frac{L}{S} = 0.005\,\frac{0.25}{1.4 \times 0.02} = 45\,\text{m}\Omega$$

with $\rho = 5\,\text{m}\Omega\,\text{cm}$ the in-plane resistivity and $S = 0.02\,\text{cm} \times 1.4\,\text{cm}$ the section of the GDL. The length L is considered equal to one quarter of the width of the cell ($L = 0.25$ cm) assuming a uniform current density in the direction perpendicular to that of the gas flows. The in-plane resistance is much lower than the contact resistance between the gold wires and the GDL (measured to 800 mΩ cm^2 per wire – 400 mΩ cm^2 per two wires) and it can be neglected.

The anodic and cathodic gas channels are parallel (Fig. 1): as a consequence, the cell can work in co-flow (air and hydrogen flow in the same direction) or counter-flow configurations (air and hydrogen flow in opposite directions). For this paper, all the experiments are performed using the co-flow configuration. The cell temperature is controlled by four water streams (Fig. 1) parallel to the gas channels. However, since PMMA is not a good conductor of heat ($\lambda = 0.17\,\text{W m}^{-1}\,\text{K}^{-1}$), local variations of the temperature occur,

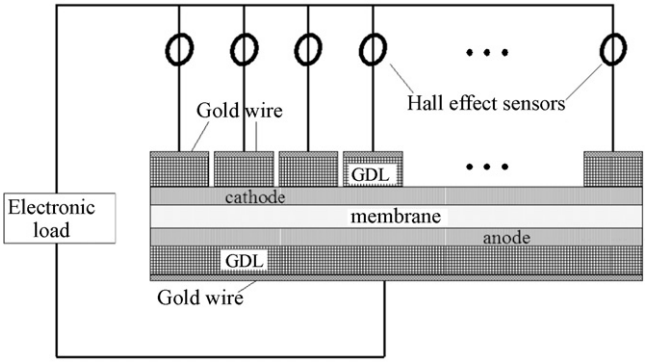

Fig. 2. Schematic of the electrical connections.

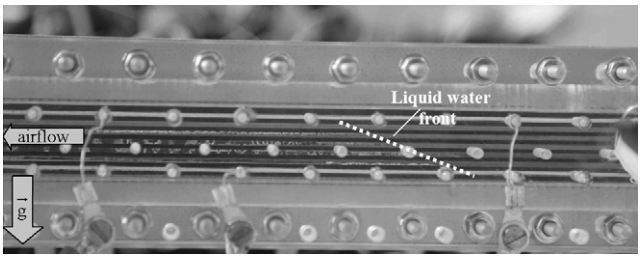

Fig. 3. Picture of the cathode side; observation of the liquid front.

which can be significant: they are measured thanks to 20 thermocouples (1 for each segment) inserted into a channel rib, as close as possible from the backing layer. In practice, it was possible to reduce to only 0.1 mm the PMMA thickness separating the end of the thermocouple from the backing layer.

The current density and temperature sensors are connected to a data acquisition and processing system allowing real-time measurements. A picture of the cathode side is presented in Fig. 3 where the appearance of liquid water in the channel can be observed. Notice that liquid does not appear at the same distance from air inlet in all channels. The membrane being positioned vertically, gravity effects explain this: there exists a liquid water flow inside the backing layer from the top to the bottom. Another remark is that PMMA is rather hydrophilic with a contact angle a little inferior to 90°. Other effects could appear with hydrophobic materials like carbon–polymer composites. They will be studied experimentally in a future work.

3. Characterization of the segmented cell

Before drawing conclusions about the non-homogeneity of the current density or temperature field, it is important to check whether the 20 segments are identical or not. In Fig. 4, the high frequency resistance (1 kHz) is plotted as a function of the segment number (number 1 corresponding to the air inlet) for two humidification temperatures. The anode is fed with the same air than the

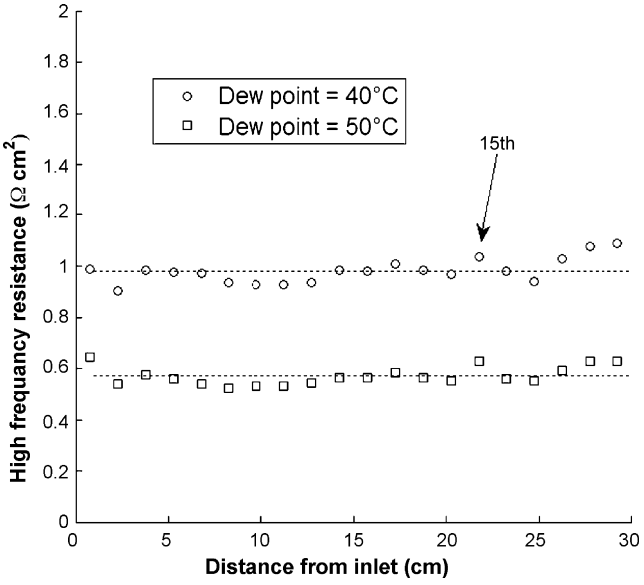

Fig. 4. High frequency resistance (1 kHz) of the 20 segments for 2 humidifying temperatures (40 and 50 °C). The cell temperature is 55 °C. Anode and cathode are both fed with moist air. Note that the contact resistance between the gold wire and the GDL is about 0.4 Ω cm².

cathode, thus there is no current or potential. The average values are 0.57 Ω cm² for medium humidification and 0.98 Ω cm² for low humidification. These values are high when compared with normal running fuel cells because of the high contact resistance (low contact surface) between the gold wires and the GDL. Standard deviations are 6% and 4%. This non-homogeneity may be due to the non-uniformity in membrane and electrodes thickness or in contact resistance between the various layers. The resistance of the 15th segment is a little more important than that of its neighbors. As shown below, this discrepancy is still observed in some cases during fuel cell operation (at high stoichiometry in Fig. 8).

4. Global observations

For these experiments, air and hydrogen are humidified with a dew point temperature of 26 °C. The flows are overheated to avoid condensation in the linking tubes. The potential is fixed to 0.5 V by an electronic load (Amrel FEL60) and the hydrogen flow remains constant ($Q_{H_2} = 3$ nL h^{-1} $S_{H_2} \approx 1.4$). The airflow rate values correspond to three different stoichiometries: $Q_{air} = 1.7$ nL min^{-1} ($S_{air} \approx 20$), $Q_{air} = 0.52$ nL min^{-1} ($S_{air} \approx 6$) and $Q_{air} = 0.17$ nL min^{-1} ($S_{air} \approx 2$). The cooling water temperature is controlled to 30 °C. The cell performance being highly correlated to its history, all the MEA were treated following the same procedure. However, as there exists non-uniformities on a single MEA (Fig. 1), discrepancies also exist between MEAs from the same batch.

The first global observations are presented in Fig. 5. Before each of the three experiments, the short time history of the cell consists in 1 h in the presence of gas flows but at zero current density, so that the humidity of membrane electrodes and gases is equilibrated. The cell is thus initially at open circuit voltage (OCV). At $t = 0$, the potential is set to 0.5 V. Fig. 5 depicts the evolutions of the average current density and temperature and of pressure loss in the air flow.

The average current density is of course sensitive to the air stoichiometry S_{air}. At very high stoichiometry ($S_{air} \approx 20$), water is evacuated by the airflow and the fuel cell hydration does not increase. However, the temperature rises as a consequence of the hydrogen oxidation and of internal electric losses within the fuel cell. The fuel cell heating is magnified by the low thermal conductivity of PMMA, which results in a drying of the MEA. As a consequence, a slight decrease in the average current density can be observed during the first minutes of operation. It is noticeable that the time constant associated with this decrease in current density corresponds to a thermal phenomenon: the evolutions of the average temperature ($S_{air} \approx 20$ and 6 in Fig. 5) show a thermal time constant of about 15 min.

At medium air stoichiometry ($S_{air} \approx 6$), the average current density is slowly increasing during a few minutes following the beginning of fuel cell operation. The temperature rise is more important than at high stoichiometry (from 30 to 42 °C instead of 31–39 °C) because of the lower amount of heat convected by the airflow. However, in spite of the higher temperature, the amount of water carried away by the airflow is lower and the fuel cell is self-humidified by the water it produces. In addition to that better humidification, the higher temperature reduces overpotentials.

This cell was designed for low pressure drop and the gas flows cannot remove properly liquid water caps that appear in the channels at low air stoichiometry ($S_{air} \approx 2$). Thus, the fuel cell is rapidly flooded in these conditions. As a consequence, correlated instabilities of the average current density and of the average temperature are observed after 15 min of operation. Fig. 5 shows that the pressure loss in the air channel is rather constant at high stoichiometry ($S_{air} \approx 20$) because of the absence of liquid water. The slight increase that is observed can be attributed to the water vapor produced and

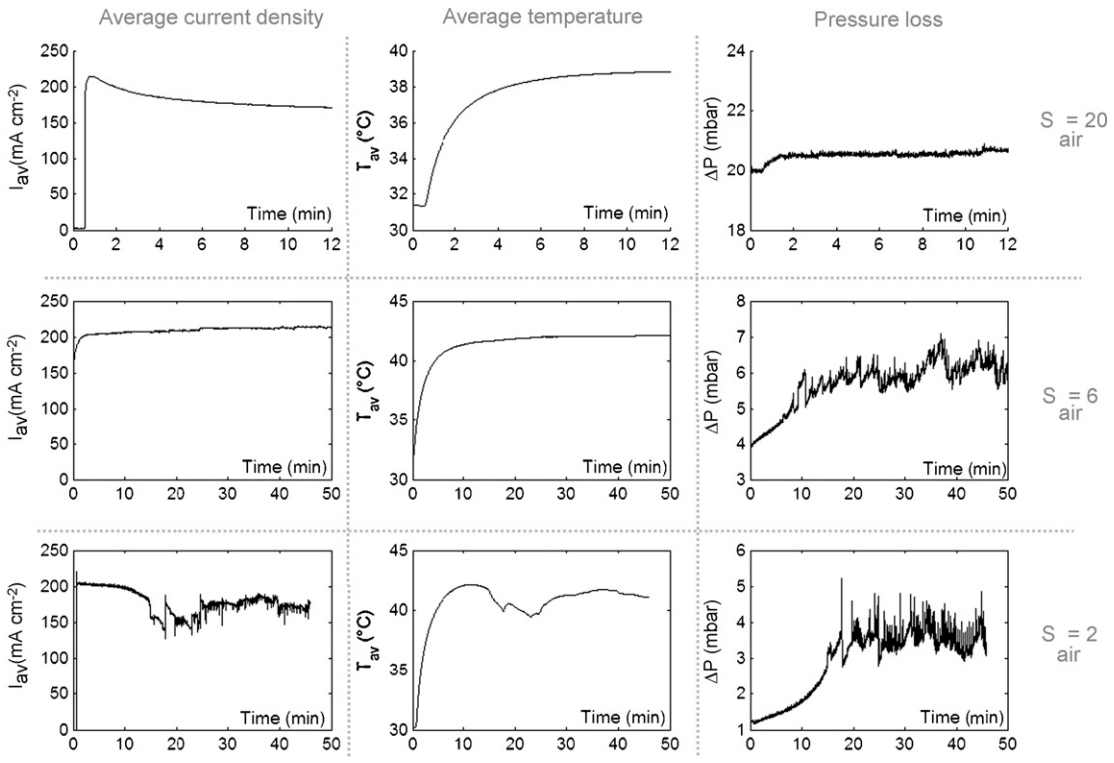

Fig. 5. Time-dependent global variables for three different stoichiometries: average current density, average temperature and cathode pressure loss.

to the temperature raise that makes the air expand. At medium and low stoichiometry, the pressure loss rises steadily until the appearance of the first liquid plug: the condensation of water reduces the hydraulic diameter. Beyond the first 10–15 min, the pressure loss shows seemingly random fluctuations around constant values, which are due to the intermittent expulsion of the liquid plugs by the airflow. Fig. 6 shows the simultaneous evolutions of the average current density and of the pressure loss in the air channel at low stoichiometry ($S_{air} \approx 2$), which illustrates explicitly the correlation between channel clogging and the electric performance of the cell.

5. Local observations

Local measurements help understanding more precisely the principles governing fuel cell performances. In this section, results of the experiments presented above (Section 4) are examined in terms of spatial variations.

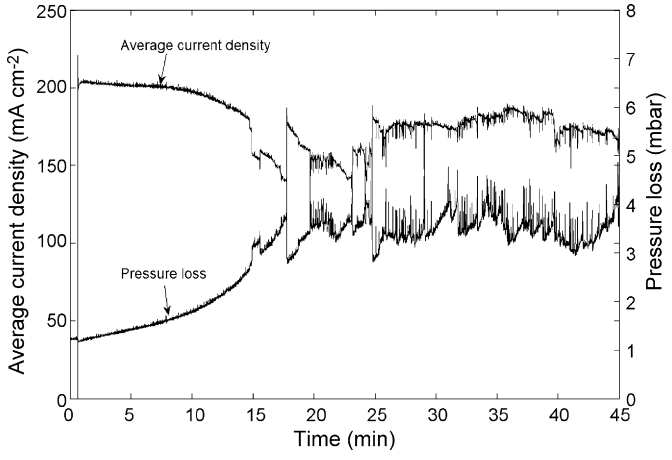

Fig. 6. Simultaneous evolutions of average current density and of pressure loss in air channel at low stoichiometry ($S_{air} \approx 2$).

5.1. Local current density and temperature field

The plots in Fig. 7 show the current densities produced by segment 2 (close to the inlet) and segment 19 (close to the outlet) as functions of time. Their evolutions can be compared to that of the average current density produced by the whole of the fuel cell.

At high stoichiometry ($S_{air} \approx 20$), the local current densities show an evolution qualitatively similar to that of the average value but with a strong difference in term of magnitude. The current density produced by segment 19 is almost twice higher than that produced by segment 2. At an air stoichiometry of 6, the inlet and outlet current densities do not show similar evolutions: at the inlet, current density decreases with time because of the temperature rise (and of the membrane drying) whereas at the outlet, the current density is increasing thanks to the cell self-humidification. Note that the temperature rise supports convective transport of vapor in the airflow by increasing the saturation pressure. Finally, at an air stoichiometry of 2, an important drop is observed at the outlet whereas the current density at the inlet remains almost constant. More precisely, small oscillations of the inlet current density occur because the downstream liquid clogs also affect the upstream flow.

Fig. 8 shows the current density and temperature profiles recorded 40 min after the beginning of fuel cell operation. As expected, at an air stoichiometry of 20, the current density is a monotone increasing function of the distance from the inlet. The dispersion observed corresponds well with the deviations of the frequency resistances plotted in Fig. 4. There is no liquid in the air channel because the airflow removes all the water by convective transport in its vapor phase. However, the air humidifies along the channel and as a result, the cathodic activation potential and

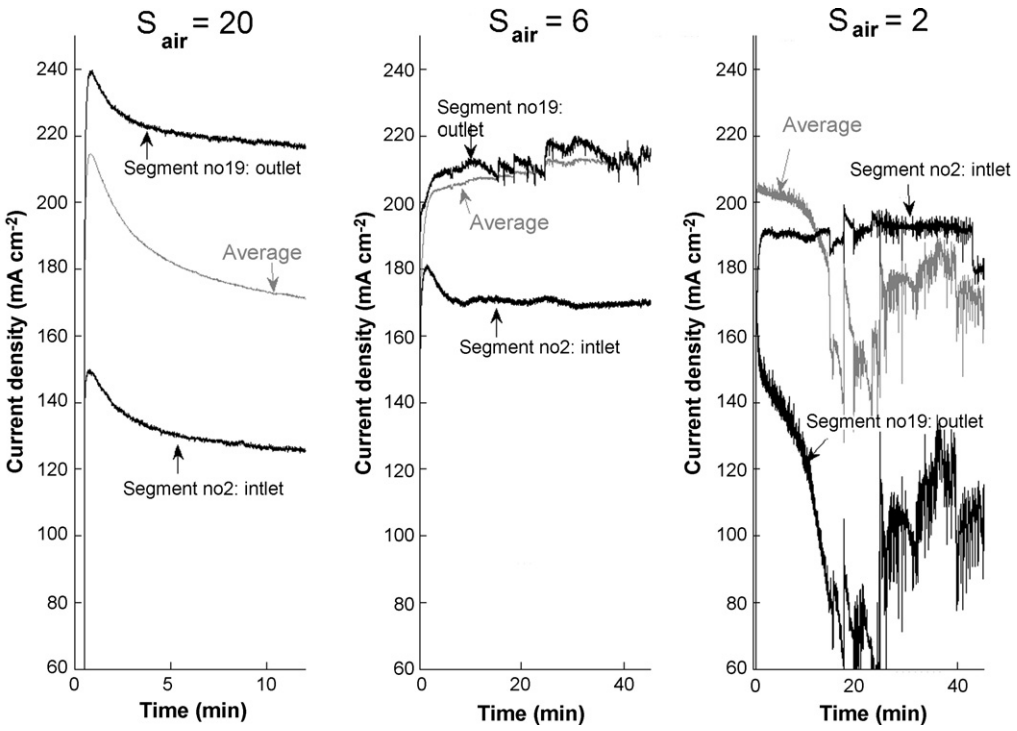

Fig. 7. Inlet and outlet current densities as functions of time for three values of the air stoichiometry.

membrane ohmic loss diminish. The temperature profile is also monotone and increasing.

At an air stoichiometry of 6, droplets are present in the air channel starting from the 8th segment as shown in Fig. 3. Then, the temperature remains rather constant before increasing again, as well as the current density, starting from the 16th segment. This rise does not seem to be explainable by the noise, so something should happen.

At an air stoichiometry of 2, liquid appears on the 2nd segment. The bell-shaped temperature and current density profiles result from dry conditions at the inlet, and from flooding (of the electrodes and/or GDL) and oxygen impoverishment at the outlet.

5.1.1. Local water balance

Temperatures reported in Figs. 5 and 8 are measured close to the interface between the backing layers and the channel ribs (the

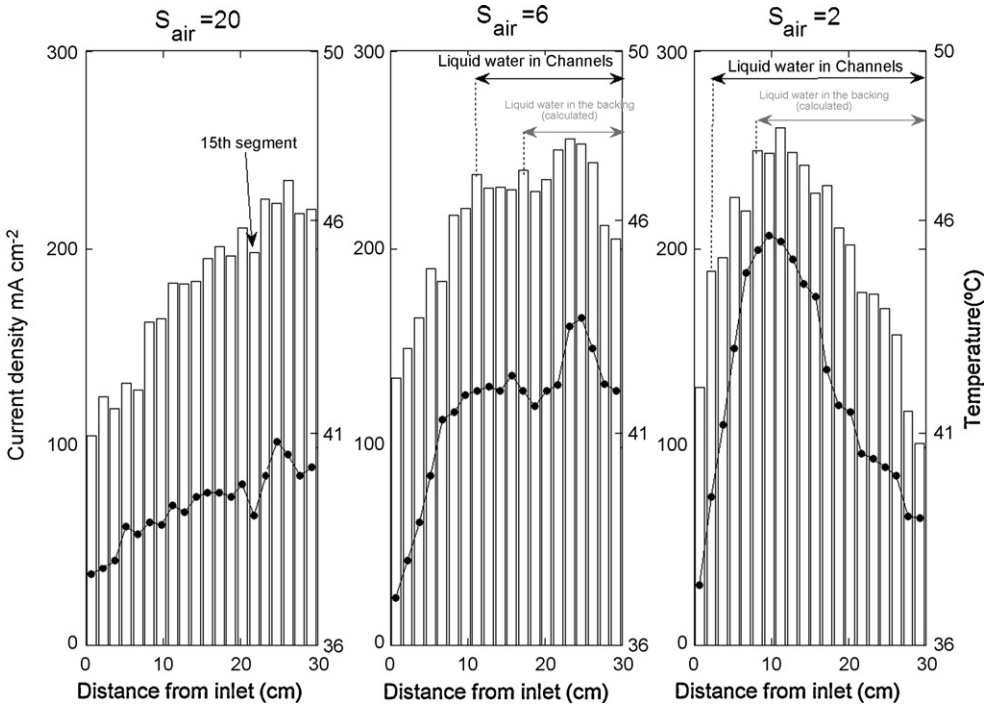

Fig. 8. Current density (bar graph) and temperature profiles at time $t = 40$ min. The location where liquid water is observed is also reported as well as the location where it should theoretically appear taking account of the measured current densities and temperature and assuming that the net drag coefficient is null.

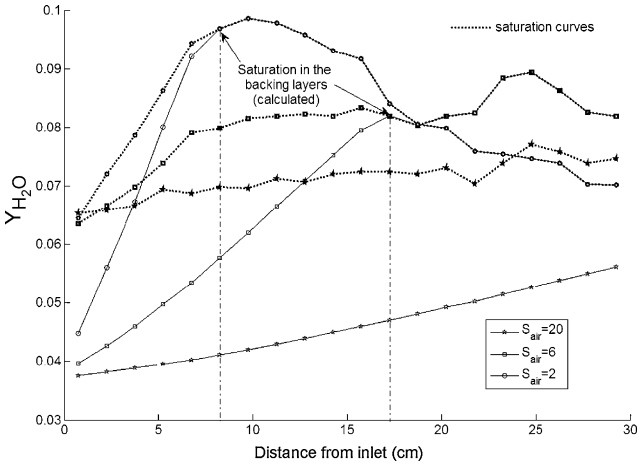

Fig. 9. Vapor local concentration and saturation concentration calculated from measured temperatures and measured current densities. The water flux through the membrane is neglected.

thermocouple solder is 0.1 mm away from the backing layer in the center of the channel rib—Section 1). The temperature of the channel wall (where water condenses) is not known. However, the knowledge of the local current density and backing layer temperature makes it possible to calculate the conditions for water condensation (in the backing layer). Considering that hydrogen is humidified and that the current density is low, it is reasonable to assume that the amount of water crossing the membrane is negligible. Consequently, the water concentration (in mole mole^{-1}) in the airflow at the outlet of segment n is given by

$$y_{H_2O}(n) = \frac{\dot{N}_{H_2O}(n)}{\dot{N}_{air}(n) + \dot{N}_{H_2O}(n)} = \frac{\dot{N}^{inlet}_{H_2O} + \Delta x \sum_{k=1}^{n} \frac{I_k}{2F}}{\dot{N}^{inlet}_{air} - \Delta x \sum_{k=1}^{n} \frac{I_k}{4F} + \dot{N}^{inlet}_{H_2O} + \Delta x \sum_{k=1}^{n} \frac{I_k}{2F}}$$

where I_n denotes the current density produced by segment n. Using the values of temperature measured on each segment T_n, the local vapor saturation concentration is expressed by the Antoine law:

$$y^{sat}_{H_2O}(n) = \exp(13.669 - 5096.23/(T(n) + 273.15))$$

The plots in Fig. 9 allow to compare values of the vapor concentration calculated as a function of current densities and those calculated as a function of the local temperature. Condensation occurs when the two curves meet.

According to the plots of Fig. 9, liquid should appear in the backing layer of segment 6 for an air stoichiometry of 2, and of segment 12 for an air stoichiometry of 6. The results confirm that the fuel cell remains dry at an air stoichiometry of 20 (the local vapor concentration stays below the saturation concentration). However, these results are only approximates because condensation on the colder face of the channel and a possible water drag through the membrane (from cathode to anode) could reduce the amount of water in the cathode backing layer: they must therefore be considered as lower bounds of the distance from inlet at which water condensates in the backing layer. The maximum current density corresponds probably with the point where the vapor saturation pressure is reached at the electrode. This could explain the slight increase in current density observed on the 16th segment at an air stoichiometry of 6 (Fig. 8). The main conclusion of this water balance is that the liquid cannot appear in the backing layer at the same distance from inlet than in the channels: there exists an area where there is liquid water in the channel but not in the backing layer. Ramousse et al. [8] also announced this result on the basis of a numerical study.

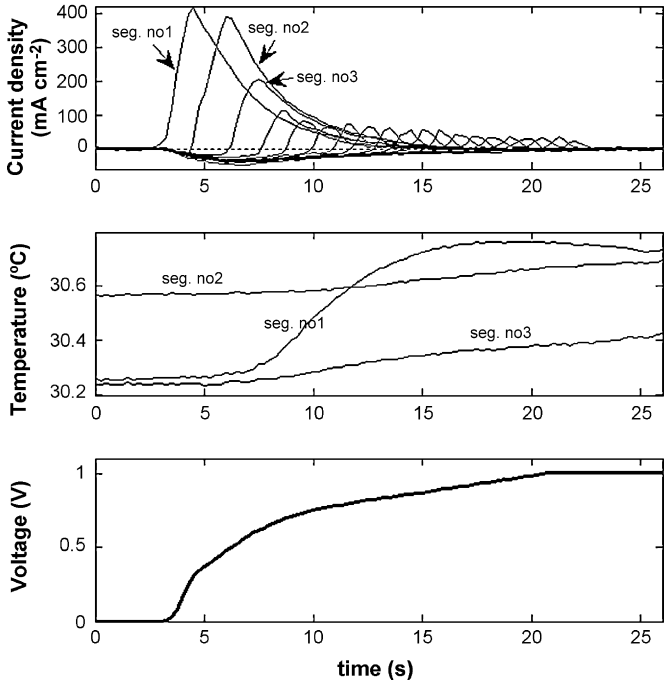

Fig. 10. Voltage rise and evolutions of local temperatures and current densities when hydrogen is introduced in an anode full of air (fuel cell at open circuit).

5.2. Local phenomena at power on: when hydrogen meets air at the anode

Hydrogen is often introduced in the fuel cell without any particular precaution, so that when it is first flowing in the anode that is full of air, internal currents and increases in temperature should occur, before or during the voltage is rising, due to the direct oxidation of hydrogen and oxygen at the anode. These phenomena are not well known but they can be investigated with a fuel cell instrumented for local temperature and current density measurements.

Some preliminary results are presented in Fig. 10. A first result is that the temperature rise is low (less than 1°), meaning that the catalyst layer and the membrane should not suffer from the direct oxidation of hydrogen in the anode at start up. Note that this result depends on the ratio of channels volume to MEA surface. This remark is valid for a hydrogen injection chamber of very low volume: the amount of oxygen consumed is practically only the one present in the channels. This is not the case when large inlet tubes are used or for a stack with a large dead volume.

However, as shown in Fig. 10, internal currents can be quite important near the channel inlet: 0.4 A cm^{-2} (maximum current density observed in Fig. 10) is a high value for this fuel cell where the contact resistances between current collectors and backing layers are significant. The 1st segment is not subject to reverse current but this is not the case of the 19 others: the sum of all currents being zero at open circuit, all the segments except the first one are subject to a reverse current and then to a positive current, which maximal intensity is decreasing from inlet to outlet. Charge storage in the double layer capacity can be mentioned as a possible explanation.

Note that the segmented fuel cell could also allows to investigate the occurrence of local currents under idle conditions (fuel cell in OCV fed by hydrogen and air). These internal currents imply water formation that could be observed in some cases. However,

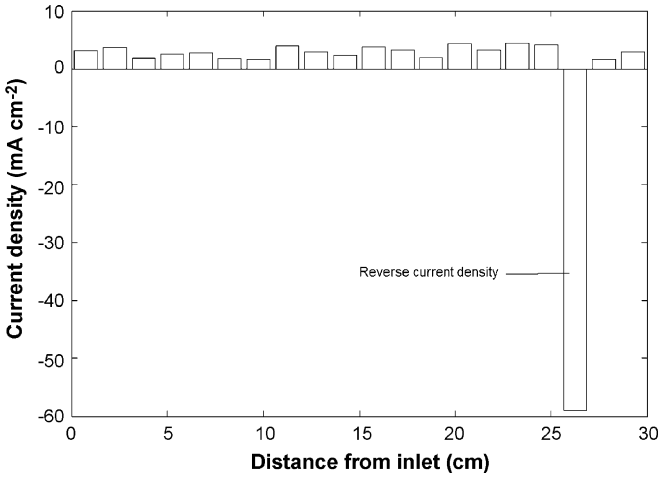

Fig. 11. Current density in open circuit conditions measured in a degraded fuel cell. $U = 0.80$ V.

these phenomena must be significant enough and they could be better studied with an optimized instrumented fuel cell with low electrical contact resistance between the GDL and the flow plates.

5.3. Local ageing effects

Fuel cell ageing results mostly from platinum migration within the membrane and from the free radical degradation of the polymer membrane. In our case, three kinds of ageing effects were observed. These results do not have statistical value because only six MEAs were tested, but it could be worth mentioning them:

(i) Sudden performance decrease of a segment linked to a raise of its high frequency resistance. This effect was observed close to the outlet where stagnant liquid water remained frequently.
(ii) Slight and progressive decrease in performance of the inlet segments without modification of their high frequency resistance. The activation losses seem to slightly increase with time when the electrodes operate in dry conditions.
(iii) Sudden decrease of the fuel cell OCV linked to a reverse current in a segment located near the outlet (Fig. 11). This reverse current density can be caused by a hole in the membrane and/or a short circuit between the two electrodes.

6. Conclusion

An experimental setup was designed to measure local current densities and the temperature field between the inlet and the outlet of a PEM fuel cell gas channels. The flow plates being made of PMMA, which is transparent, an additional observable is the location where liquid water appears in the channels. A parallel was made between global and local observations: in particular, instabilities in the fuel cell performances (whether expressed in term of variations in the mean current density at constant cell voltage or in term of voltage variations at constant current intensity) seem to be directly related to the intermittent expulsion of the liquid plugs by the airflow. Among the main results, it also appears that the temperature field is strongly correlated with the current density distribution and both depend strongly on water management. Some local aging effects are reported, as well as the observation of internal currents in open circuit conditions when hydrogen is flowing first in the anode channel. These internal currents can reach high intensity, which may have consequences on reliability.

References

[1] S.J.C. Cleghorn, C.R. Derouin, M.S. Wilson, S. Gottesfeld, J. Appl. Electrochem. 28 (1998) 663–672.
[2] D.J.L. Brett, S. Atkins, N.P. Brandon, N. Vasileiadis, V. Vesovic, A.R. Kucernak, J. Power Sources 172 (2007) 2–13.
[3] J. Stumper, S.A. Campbell, D.P. Wilkinson, M.C. Johnson, M. Davis, Electrochim. Acta 43 (24) (1998) 3773–3783.
[4] M.M. Mench, C.Y. Wang, M. Ishikawa, J. Electrochem. Soc. 150 (2003) A1052–A1059.
[5] H. Sun, G. Zhang, L. Guo, H. Liu, J. Power Sources 158 (2006) 326–332.
[6] M. Schulze, E. Gulzow, St. Schonbauer, T. Knori, R. Reissner, J. Power Sources 173 (2007) 19–27.
[7] G. Maranzana, O. Lottin, S. Didierjean, Proceedings of the Hydrogen & Fuel Cell 2007, International Conference and Trade Show, Vancouver Convention & Exhibition Centre, Vancouver BC, Canada, April 29–May 2, 2007, pp. 460–469.
[8] J. Ramousse, J. Deseure, S. Didierjean, O. Lottin, D. Maillet, J. Power Sources 145 (2) (2005) 416–427.